RSC Advances

PAPER

View Article Online
View Journal | View Issue

Cite this: *RSC Adv.*, 2016, **6**, 29279

A facile one-step method to synthesize SiO_2@polydopamine core–shell nanospheres for shear thickening fluid†

Mei Liu,[a] Wanquan Jiang,*[a] Qian Chen,[b] Sheng Wang,[a] Ya Mao,[a] Xinglong Gong,*[b] Ken Cham-Fai Leung,[c] Jie Tian,[d] Huijuan Wang[d] and Shouhu Xuan*[b]

Received 3rd December 2015
Accepted 18th February 2016

DOI: 10.1039/c5ra25759j

www.rsc.org/advances

A facile one-step method was developed to synthesize core–shell structured SiO_2@polydopamine (PDA) nanospheres. During the synthesis, a PDA shell was simultaneously coated on the SiO_2 nanospheres to form the core–shell nanostructure. The PDA shell thickness was tunable by varying the concentration of the starting dopamine precursor. After dispersing the core–shell nanospheres into poly(ethylene glycol) 200 (PEG200), a SiO_2@PDA based shear thickening fluid (STF) was obtained. In comparison to pristine SiO_2, the SiO_2@PDA based STF presented better ST effects and its maximum viscosity could reach as high as 194.6 Pa s. A possible enhancement mechanism was proposed in order to investigate the structural dependence of the ST effect. This high performance SiO_2@PDA based STF could be widely applied in body armor and other safe-guarding areas.

1. Introduction

Shear-thickening (ST) is a type of non-Newtonian flow behavior in concentrated suspensions, where the viscosity increases dramatically when encountering an unexpected force. If the applied shear or striking is beyond the critical value, the fluid becomes thicker and can even transform from the liquid state to a solid-like state.[1–4] Due to this unique reversible ST effect, ST fluids (STFs) have attracted attention for a wide array of applications such as dampers, "liquid" armor, impact absorbers, control devices, sports shoe cushioning, rotary speed limiters, *etc.*[4–7] It has been claimed that shear thickening originates from hydrodynamic lubrication forces between the dispersed particles.[8–11] Various techniques such as rheo-optical and neutron scattering, flow-ultra small angle neutron scattering, and fast confocal rheology measurements have been used to support the above mechanism.[9,10,12,13]

During the past few decades, much effort has been expended on the preparation of high performance STFs and investigation of their structure dependent rheological properties. Previous work has indicated that the mechanical characteristics of STFs are influenced by the dispersing particles, the carrier fluid, and any additives.[14–20] Among these, the dispersing particles play a critical role. A large number of natural materials such as calcium carbonate, silica, alumina, titania, barium sulfate,[21] blood cells, cornstarch particles,[4] and starch particles[22] have been effective for STFs. Recently, in order to obtain high performance STFs, man-made particles such as poly(vinyl chloride) (PVC), poly(styrene-acrylonitrile) (PS-AN), polystyrene (PS)],[4] poly(methyl methacrylate) (PMMA),[12] poly(styrene-ethyl acrylate) (PS-EA),[23] and carbon nanofibers[24] have been introduced into the ST area. Due to their tunable hardness, charge and elastic surfaces, these particles have become attractive for use in STFs as these properties usually result in strong ST behavior.[23]

The characteristics of the particles play an important role in determining the ST effect.[25] As soon as the yield strain is reached, the hard particles collide with each other and this leads to shear thickening. However, the shear thickening is damped by the thick outer shells of soft particles.[26] Recently, our group investigated the influence of the particle structure on the behavior of STFs by synthesizing PS-AA (polystyrene-acrylic acid) nanospheres with different structures. We found that particles with a proper hard core and a soft shell exhibited excellent shear thickening behavior.[27] The soft shell contributed to an increase in the hydrodynamic lubrication interactions between the dispersing particles, which resulted in particle clusters being formed much more easily. The hard cores of the nanospheres ensured the formed clusters could resist a larger imposed stress. Therefore, it was proposed that the ideal

[a]*Department of Chemistry, Collaborative Innovation Center of Suzhou Nano Science and Technology, University of Science and Technology of China (USTC), Hefei 230026, PR China. E-mail: jiangwq@ustc.edu.cn; gongxl@ustc.edu.cn; xuansh@ustc.edu.cn; Fax: +86-551-63600419; Tel: +86-551-63607605*

[b]*CAS Key Laboratory of Mechanical Behavior and Design of Materials, Department of Modern Mechanics, USTC, Hefei 230027, PR China*

[c]*Department of Chemistry and Institute of Creativity, Hong Kong Baptist University, Kowloon, Hong Kong SAR, P. R. China*

[d]*Engineering and Materials Science Experiment Center, USTC, Hefei 230027, PR China*

† Electronic supplementary information (ESI) available. See DOI: 10.1039/c5ra25759j

dispersing particle for a high performance STF should possess a hard core and a soft shell.[4,27]

Core–shell particles are of specific research interest because they can integrate two or three different functionalities together into one material.[28,29] During the past decade, various core–shell particles such as the inorganic core/inorganic shell, inorganic core/polymer shell, and polymer core/polymer shell have been reported for applications in biology, energy, separation, catalysis *etc. In situ* coating,[30,31] layer by layer,[32–34] and one-pot methods are the most favorable methods for preparing core/shell nanospheres.[35–37] Due to the incompatibility between the inorganic material and the polymer, complicated procedures[38,39] have often been required to fabricate core–shell particles with an inorganic core/polymer shell. Moreover, the scale of traditional methods for the synthesis of core/shell nanospheres is usually small.[39,40] Typically, in previous works about preparation of core–shell particles, the scale of the products is small and the maximum scale does not exceed 5 g.[41–45] However, the scale of particles required for use in STFs is relatively large. Therefore, a facile one-step method for preparing inorganic/polymer nanospheres would be useful for STFs.

Hard SiO_2 nanospheres are usually used in STFs due to their easy preparation and tunable size. Many works have been carried out on the development of polymer coated SiO_2 nanospheres, such as SiO_2@poly(methyl methacrylate) (PMMA),[46–48] SiO_2@polystyrene (PS),[49] SiO_2@poly(3-aminophenylboronic acid),[50] and SiO_2@poly(vinyl chloride) (PVC).[51] Unfortunately, although many works have been carried out on the development polymer encapsulated SiO_2 nanospheres, there is still no report about the one-step fabrication of the SiO_2@polymer core–shell particles and the subsequent investigation of their STFs.

In this work, a one-step approach has been developed to scale-up the synthesis of SiO_2@polydopamine (PDA) inorganic–organic core/shell nanospheres. The thickness of the PDA shell was tunable by varying the concentration of the dopamine precursor. By dispersing the SiO_2@PDA core/shell nanospheres into PEG200, the related STFs were obtained and they exhibited larger ST effects than a SiO_2 based STF. A possible improvement mechanism was proposed and it was found that the PDA shell played a critical role in decreasing the critical shear rate. The as-prepared high performance STF could be widely applied in dampers and impact absorbers.

2. Experimental

2.1. Materials

Tetraethylorthosilicate (TEOS), ethanol and ammonium hydroxide ($NH_3 \cdot H_2O$, 25–28%) were purchased from Sinopharm Chemical Reagent Co. 3-Hydroxytyramine hydrochloride (98%) was purchased from Aladdin. All chemicals were used directly as received without further treatment. Re-distilled water was used in this work.

2.2. The preparation of SiO_2@PDA nanospheres

Scheme 1 illustrates the preparation process of the nanospheres. The synthesis was conducted in a 2000 mL three necked flask, which was fitted with a mechanical stirrer. Ethanol (1142 mL), distilled water (49.3 mL) and ammonium hydroxide (93.2 mL) were added to the flask and the mixture was stirred for 10 min. TEOS (53.6 mL) was then added into the solution dropwise. After 4 h, TEOS (26.8 mL) and distilled water (24.7 mL) were added into the solution. 8 h later, TEOS (26.8 mL) and distilled water (24.7 mL) were added into the solution again. The temperature was kept at 40.3 °C by using a Thermostatic Water Bath. 8 h later, a specified amount of dopamine was introduced into the reaction solution and the reaction was maintained at 25 °C for 24 hours. SiO_2@PDA core/shell nanospheres with different PDA layer thicknesses were prepared by varying the dopamine concentration to 1.0 g L^{-1} (SiO_2@PDA-1), 2.0 g L^{-1} (SiO_2@PDA-2), 3.0 g L^{-1} (SiO_2@PDA-3) and 4.0 g L^{-1} (SiO_2@PDA-4). The resultant SiO_2/PDA nanospheres were collected by centrifugation after polymerization. After being rinsed with ethanol and distilled water three times, the product was dried in a vacuum oven at 50 °C.

2.3. The preparation of the SiO_2@PDA based STFs

Firstly, the SiO_2@PDA nanospheres were added into PEG200. The mixture was then mixed in a ball crusher in order to obtain a homogeneous dispersion. 24 h later, the final product was collected when no large-scale aggregation was found in the suspension. The obtained STF was sealed in a vial before use.

2.4. Rheological measurements

The rheological properties of the STFs were measured using a rheometer (Physical, MCR301, Anton Paar) at 25 °C with a cone-plate having a cone angle of 0.2° and a diameter of 25 mm. The rheological properties of each sample were measured under both static and dynamic loading conditions. The steady-shear and oscillatory-shear tests were conducted with a gap size of 0.05 mm. In order to remove loading effects, a pre-shear of 1 s^{-1} was applied for 60 s before collecting the experimental data.

2.5. Characterization

The particle size and macroscopic features were determined by a field emission scanning electron microscope (20 kV, JEOL JSM-6700F SEM). The thickness of the shell was observed using transmission electron microscopy (TEM, JEM-2011) with an accelerating voltage of 200 kV. Infrared (IR) spectra were measured using a Nicolet Model 759 Fourier transform infrared (FT-IR) spectrometer in the wavenumber range 4000–500 cm^{-1} with a KBr wafer. X-ray photoelectron spectra (XPS) were measured on an ESCALAB 250. Thermogravimetric (TG) analysis was performed in air from room temperature to 700 °C at the rate of 10 °C min^{-1} on a DTG-60H thermogravimetric instrument.

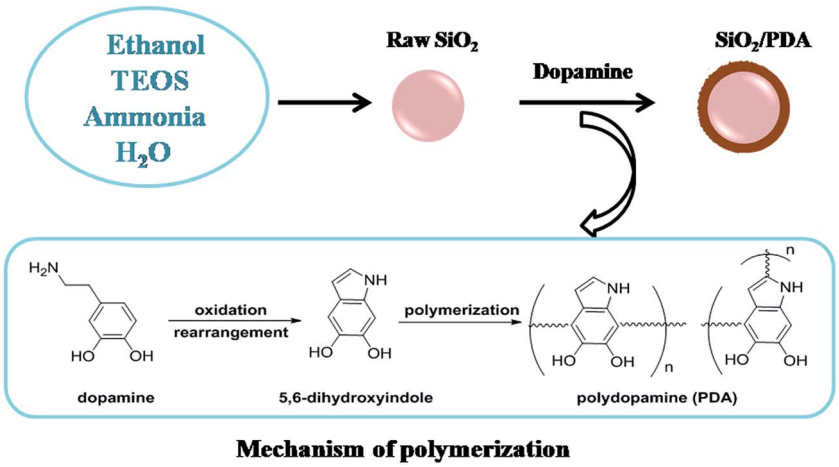

Scheme 1 An illustration of the synthesis of SiO_2@PDA core/shell nanospheres and the proposed mechanism.

3. Results and discussion

3.1. Preparation and characterization of the SiO_2@PDA nanospheres

In this one-step synthesis, the SiO_2@PDA nanospheres were obtained using a modified Stöber reaction. Firstly, SiO_2 nanospheres were formed during the hydrolysis of the TEOS precursor in the alkali medium. As soon as the TEOS was almost completely consumed, the dopamine was added into the solution to coat a PDA layer onto the surface of the SiO_2 nanospheres. After rinsing and vacuum heating, SiO_2@PDA particles were obtained. Due to the simplicity and green nature of the process, this economical method is of high potential value for practical applications.

Fig. 1a shows a SEM image of the SiO_2@PDA product prepared with a DA concentration of 2 g L^{-1}. All of the particles possessed a spherical morphology and were well dispersed without any large-scale aggregation. These nanospheres were uniform and the average size was about 360 nm. TEM was applied to investigate the inner nanostructure of the SiO_2@PDA nanospheres. Interestingly, besides the black core, there was a thin layer covering the surface of the nanosphere, which indicated that the SiO_2@PDA nanospheres possessed a typical core/shell nanostructure (Fig. 1b). A higher magnification TEM image showed that the shell thickness was about 10 nm (Fig. 1d). Considering that the DA monomer was added later, the thin shell was thought to be the PDA. Fig. 1c shows a photo of the SiO_2@PDA nanospheres prepared in one of the experiments. The yield of the nanospheres was 32 g in a one-pot reaction, which is much larger than most of the previous methods for preparing core/shell nanospheres. Moreover, due to the PDA shell, the powder was gray in color, which was different from the white pristine SiO_2.

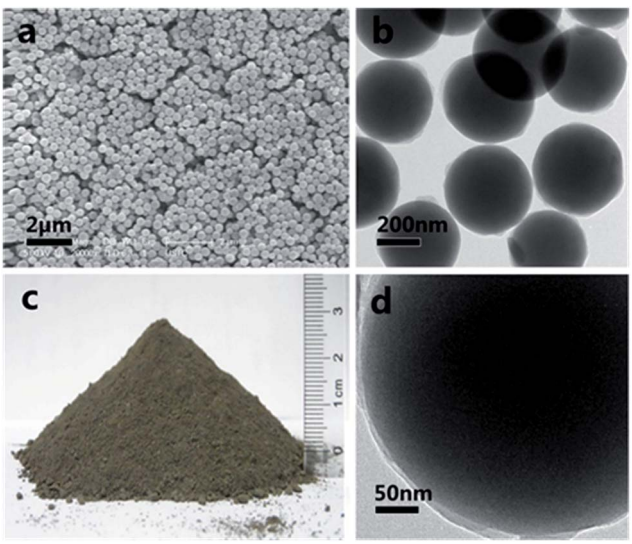

Fig. 1 SEM (a) and TEM (b and d) images of the SiO_2@PDA nanospheres synthesized with dopamine concentration of 2 g L^{-1}; (c) shows a photograph of the one-pot product.

Since it has a hydrophilic surface, the PDA can attach to the SiO_2 nanospheres to form a core–shell nanostructure. With an increase in the DA concentration, the PDA shell thickness increased. Fig. 2a–l shows SEM and TEM images of pristine SiO_2 (a–c) and the SiO_2@PDA (d–l) nanospheres. Without the PDA coating, all of the SiO_2 particles were spherical and the average size was about 350 nm. A thin layer appears on the surface of the SiO_2 when the PDA is polymerized *in situ*. PDA is a low molecular weight polymer and it exhibits lower contrast than the SiO_2, thus it is difficult to distinguish the shell when the shell thickness is thin. Although it is hard to observe the thin PDA shell in the TEM images, the shell is indeed coated on the SiO_2 surface because the powder is gray in color. Energy dispersive spectrometry (EDS) mapping spectra of each element on the surface of the SiO_2@PDA core–shell nanoparticles indicated that the layer of polydopamine was encapsulated on the surface of SiO_2 (Fig. S2†). Additionally, with an increase in the shell thickness, the PDA layer could be clearly observed in the TEM image. In this work, the starting concentration for dopamine was controlled from 1 g L^{-1} (d–f) to 3 g L^{-1} (g–i), then 4 g L^{-1} (j–l). The TEM images indicated that the average shell thickness

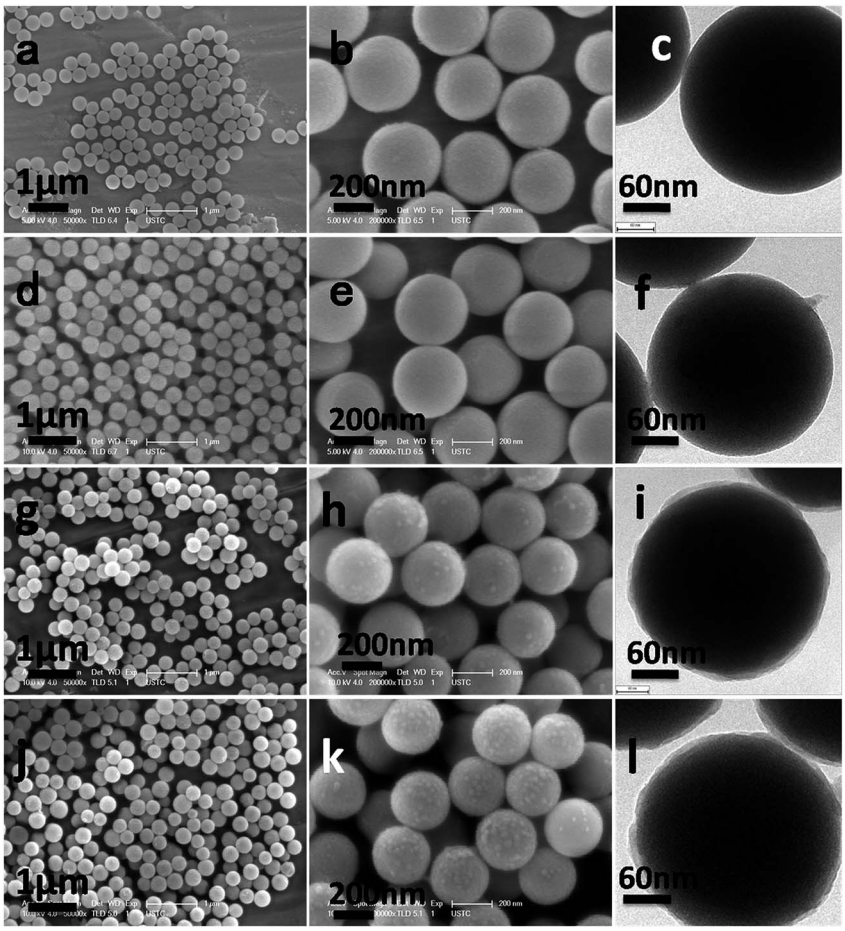

Fig. 2 SEM (a, b, d, e, g, h, j, k) and TEM (c, f, i, l) images of the SiO_2 (a–c) and SiO_2@PDA nanospheres synthesized with dopamine concentrations of 1 g L^{-1} (d–f), 3 g L^{-1} (g–i) and 4 g L^{-1} (j–l).

increased from 2 nm to 13 nm. In contrast to the smooth SiO_2, the surface of the SiO_2@PDA particles became rough, which corresponded to the PDA shell. Importantly, the PDA shell was uniformly coated on the SiO_2 nanospheres without shell coalescence, thus the obtained product was monodisperse (Fig. S1†).

The FTIR spectra of polydopamine, pristine SiO_2 and SiO_2@PDA nanospheres were investigated. Fig. 3a shows the typical FT-IR spectra of polydopamine, which has broad bands in the range between 940 and 1800 cm^{-1} with no distinguishable peaks due to the highly complex structure of polydopamine. The peaks centered at around 3346 cm^{-1} can be ascribed to the stretching vibrations of the nitrogen–hydrogen (–NH)/oxygen–hydrogen (–OH) bonds. Due to the low content of PDA, the SiO_2 (Fig. 3b) and SiO_2@PDA (Fig. 3c) nanospheres possess similar FTIR spectra. For the SiO_2@PDA nanospheres, the strong absorptions located at 1104 cm^{-1} and 804 cm^{-1}, could be assigned to the stretching vibrations of the silicon–oxygen (–Si–O–) bonds.

XPS spectra were employed to analyze the surface of the final product. Typically, strong O1s and Si2p peaks were clearly found in the spectra of the SiO_2 nanospheres (Fig. 4a). A tiny C1s peak was present in the spectra, which may be due to residual ethanol or $–OCH_2CH_3$ groups on the surface of the SiO_2 nanospheres. For the SiO_2@PDA core–shell nanospheres, a distinctive nitrogen signal can be clearly observed in Fig. 4b. The molar ratio of nitrogen (N1s, 401.8 eV) on the surface of the SiO_2@PDA nanospheres was 7.88%. Moreover, the intensity of

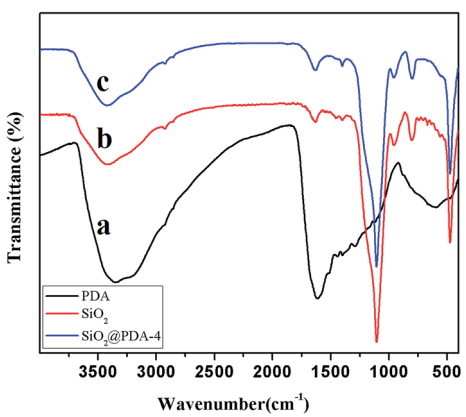

Fig. 3 FTIR spectra of (a) polydopamine, (b) pristine SiO_2 particles and (c) SiO_2@PDA particles synthesized with a dopamine concentration of 4 g L^{-1}.

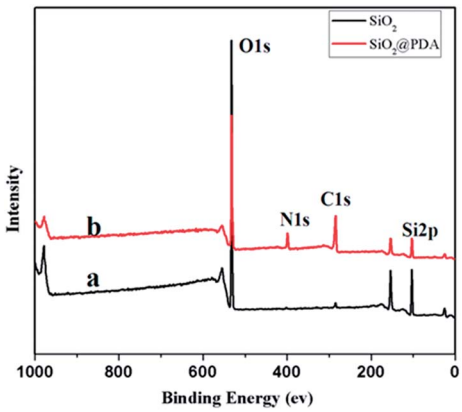

Fig. 4 Broad-range XPS spectra of SiO_2 (a) and the SiO_2@PDA (b) nanospheres.

the C1s peaks was also obviously enhanced. The detective depth of the XPS is about 10 nm and the shell thickness of the PDA is thinner, thus a Si2p signal was also present in the SiO_2@PDA nanospheres spectra. These results demonstrate the successful coating of the PDA shell onto the SiO_2 nanospheres because the N1s and C1s signals in the XPS spectra mainly arise from the PDA, which contains large number of amide and benzyl functional groups.

Shown in Fig. 5a is the thermogravimetric curve of pristine SiO_2. The weight loss observed from 0 to 100 °C could be attributed to adsorbed water. With a further increase in temperature to 500 °C, a slow weight loss was observed, which corresponded to residual organic groups in the SiO_2 nanospheres. This result also agreed with the XPS analysis. For SiO_2@PDA (Fig 5b and c), the weight loss in this area clearly increased and this could be attributed to the decomposition of the PDA. The gradual weight losses observed for the SiO_2 nanospheres (a), SiO_2@PDA-2 (b) and SiO_2@PDA-4 (c) were 11.2%, 15.4% and 19.9%, respectively. The different weight losses observed between the SiO_2@PDA-2 and SiO_2@PDA-4 nanospheres indicated that they had different PDA content in their shells. The weight loss increased with increasing thickness of the coated layer. In order to give an accurate value for the density of the nanospheres, we performed solution (double-stilled water) densitometry measurements at different mass fractions by means of a pycnometer. The results indicated that the density of the SiO_2 nanospheres was 2.05 ± 0.01 g cm^{-3}, while SiO_2@PDA-2 was 1.94 ± 0.01 g cm^{-3} and SiO_2@PDA-4 was 1.89 ± 0.01 g cm^{-3} (278 K). The average density of the SiO_2@PDA core–shell particles was slightly less than the SiO_2.

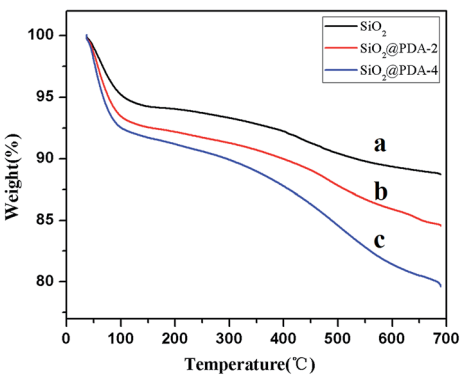

Fig. 5 TG of the as prepared (a) SiO_2 particles, as well as the (b) SiO_2@PDA-2, and (c) SiO_2@PDA-4 nanospheres.

3.2. The ST rheology behavior of the SiO_2@PDA nanosphere-based STFs

After dispersing the SiO_2@PDA core/shell nanospheres into the PEG200 solvent, the dark brown STF was obtained. A picture of the STF is shown as an inset in Fig. 6. Clearly, the STF has good fluidity and the core/shell particles are uniformly dispersed within the carrying fluid without any large-scale aggregation. Fig. 6 shows the static rheological properties of the SiO_2@PDA nanosphere-based STFs (58 wt%), in which the SiO_2@PDA nanospheres have different shell thicknesses. To better understand the effect of the PDA shell, a SiO_2 nanosphere-based STF was also prepared. Due to the low mass fraction of 58%, no obvious ST behavior was found in the SiO_2 nanosphere-based STF. However, as shown in Fig. 6, the SiO_2@PDA-1 based STF presented typical ST behavior and its maximum viscosity could reach 26.2 Pa s. Interestingly, the maximum viscosity of the SiO_2@PDA nanosphere-based STFs increased with the thickness of the PDA shell. Moreover, the critical shear rate decreased with increasing PDA shell thickness and could decrease to nearly 1 or 2 s^{-1}. Unfortunately, the initial viscosity of the STFs increased from 5.2 to 12.1, then 51.2, and 64.8 Pa s while the relative maximum viscosity was 26.2, 51.6, 86.4, and 90.4 Pa s, respectively. The SiO_2@PDA-2 based STF had the largest relative increased in viscosity (about 400%), thus SiO_2@PDA-2 was considered to be the optimum candidate for a high performance STF.

The influence of the shell thickness on the rheological behavior of the related STF was performed by using SiO_2@PDA-2 as an example. Fig. 7 shows the static rheological properties of

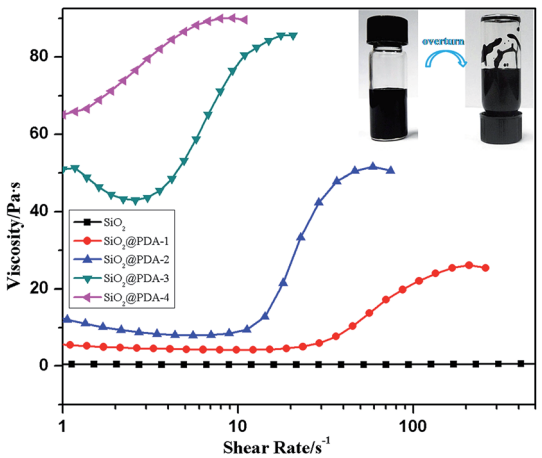

Fig. 6 Viscosity *vs.* shear rate under steady shear mode for the SiO_2 and PDA@SiO_2 nanosphere-based STFs. The inset picture illustrates the good fluidity of the PDA@SiO_2 nanosphere-based STFs.

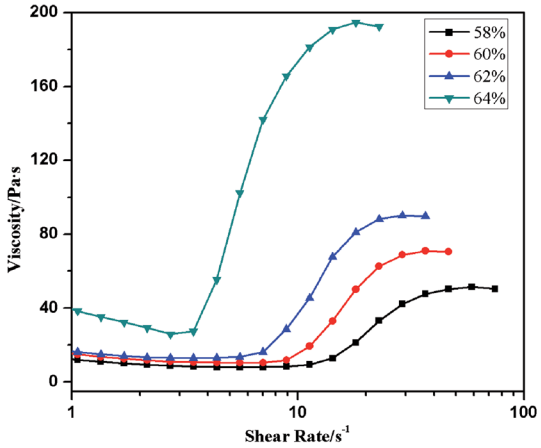

Fig. 7 Viscosity *vs.* shear rate for different mass fraction (64%, 62%, 60% and 58%) suspensions of SiO_2@PDA-2 under steady shear mode.

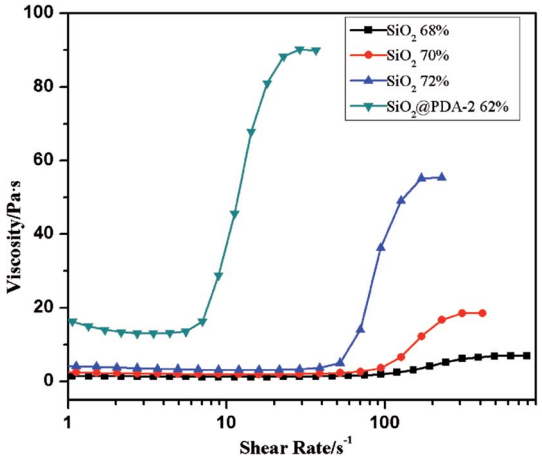

Fig. 8 Viscosity *vs.* shear rate for SiO_2 nanosphere-based STFs with different mass fractions (68%, 70% and 72%) and the SiO_2@PDA-2 based STF (62%).

SiO_2@PDA-2 based STFs containing different mass fractions (64%, 62%, 60% and 58%). It can be observed that the viscosity curve becomes steeper and the maximum viscosity in the ST region increases with increasing concentration. When the mass fraction is 58%, the critical shear rate and the maximum viscosity are 12.8 s^{-1} and 51.6 Pa s, respectively. Once the mass fraction reaches 64%, the critical shear rate decreases to 2.5 s^{-1} and the maximum viscosity can reach up to 194.6 Pa s. The critical shear rate is reduced by 5 times, approximately, while the maximum viscosity increases by about 4 times.

The above results indicated that the critical shear rate was highly dependent on the mass fraction. As the mass fraction increases, the critical shear rate decreases. At the same time, the initial viscosity increases with increasing mass fraction. When the mass fraction increased from 58% to 64%, the initial viscosity increased from 12.1 Pa s to 35.3 Pa s. Particle concentration is one of the most important factors in controlling the ST behavior of suspensions. Under shear loading, the dispersed particles are pushed into each other. They must overcome the viscous drag forces derived from the small lubrication gaps between neighboring particles so as to form a hydrocluster. At a high concentration, the average distance between two adjacent particles would be shortened and the hydrodynamic forces would make it easier to move more particles to form larger particle clusters. As a result, the critical shear rate decreases and ST effect enhances as the particle concentration is increased.

In order to further compare the different rheological properties of the SiO_2 and SiO_2@PDA nanosphere-based STFs, the influence of the mass fraction on the SiO_2 nanosphere-based STF was also investigated. Fig. 8 shows that the maximum viscosity was 7.3 Pa s, 18.6 Pa s and 55.3 Pa s when the mass fraction was 68%, 70% and 72%, respectively. Similar to the SiO_2@PDA based STFs, the critical shear rate of the SiO_2 based STF decreased from 155.5 s^{-1} to 95.3 s^{-1}, and then 52.9 s^{-1}. In contrast, the maximum viscosity and critical shear rate of the SiO_2@PDA-2 based STF with a mass fraction of 62% are 90.1 Pa s and 5.7 s^{-1}, respectively. It is worth mentioning that the initial viscosity of the SiO_2@PDA-2 based STF (16.1 Pa s) is higher than the pristine SiO_2 nanosphere-based STF (by approximately 3 Pa s). Generally, the SiO_2@PDA-2 based STF exhibits better rheological behavior than the SiO_2 nanosphere-based STF even though the concentration is lower, which demonstrates that the PDA coating layer on the surface of the SiO_2 nanospheres improves the rheological behavior of the STFs.

In this work, the reproducibility of shear thickening performance under cyclic loading was investigated. Fig. 9 shows the viscosity of the SiO_2@PDA-2 based STF with a mass fraction of 62% measured for both ascending and descending shear rate sweeps. There is a slight decrease in viscosity at a low shear rate, while it increases quickly as soon as the shear rate reaches the critical shear rate. At the same time, the viscosity decreases immediately when the shear rate decreases. It should be noted that the viscosity measurements are in good agreement at the same shear rate, which indicates that the shear thickening behavior of the SiO_2@PDA-2 based STF is reversible. The hydroclusters formed in the shear thickening period can

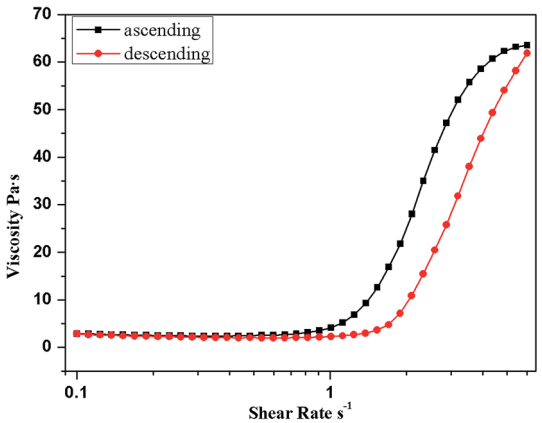

Fig. 9 Reversible shear thickening behavior of the SiO_2@PDA-2 based STF with a mass fraction of 61%.

decompose and disperse in the dispersed phase again as soon as hydrodynamic lubrication is decreased.[4] To this end, we can conclude that the as-prepared shear thickening fluid exhibits excellent cyclic reversibility in it ST effect, which is very beneficial for industrial applications.

3.3. The enhancement mechanism for the SiO_2@PDA nanosphere- based STFs

Based on the above analysis, it was found that SiO_2@PDA is superior to the naked SiO_2 when used in STFs, thus the effect of the PDA shell is important for understanding the improvement mechanism. It is known that PDA contains a large number of hydrophilic hydroxyl and amino groups (Scheme 1). Due to these hydrophilic groups, PDA is compatible with the surface of SiO_2. As the density of PDA is lower than SiO_2, the stability of the SiO_2@PDA particles in the suspension must be much better. Moreover, due to the large number of hydroxyl and amino groups on the surface, the SiO_2@PDA core–shell particles show higher affinity to the PEG solvent than the naked SiO_2 particles. Moreover, it is well known that the hardness of PDA is lower than SiO_2. After coating with a PDA shell, the obtained SiO_2@-PDA core–shell particles possess a hard core and a soft shell. The soft PDA shell enhances the hydrodynamic lubrication interactions between the core–shell particles, thus favoring the formation of particle clusters when the suspension is subjected to shear.[27]

According to the hydrocluster mechanism (Scheme 2), random collisions among particles make them naturally resistant to flow in order to maintain an equilibrium state. Under the application of external shear stress (or the shear rate), the particles become organized in the shear flow, which lowers the viscosity and, therefore, shear thinning occurs. If the shear rate reaches a critical value, the hydrodynamic interactions between particles occupy the main position and leads the random dispersion of particles to spawn hydroclusters (Scheme 2, orange). In this case, the suspension presents a transient fluctuation, thus the viscosity abruptly increases. This phenomenon is named shear thickening. The surface properties of the dispersed particles play an important role in the rheology of the dense suspension.[2,52,53] It is well known that there are large numbers of hydrophilic hydroxyl and amino groups in PDA. The PDA layer can be used as an intermediate to anchor functional molecules onto the surface through chemical bonds or other physical bonds (such as hydrogen bonds or van der Waals' forces), which indicates that the surface of the PDA layer is abundant with hydroxyl and amino groups.[54–56] Hydroxyl groups and amino groups can form hydrogen bonds with certain polar molecules.[57,58] It is rational to speculate that hydrogen bonds have been formed between the nanospheres and the PEG200. Furthermore, the interactions of hydrogen bonds are commonly found in explanations of the mechanism of shear thickening.[53,59] In SiO_2@PDA core–shell nanoparticle-based STF, due to the large number of hydroxyl groups on the particle surfaces, the particle interactions are enhanced by hydrogen bonds between particles. Therefore, hydroclusters formed in the SiO_2@PDA core–shell nanoparticle-based STF must be larger than in the SiO_2 based STF.

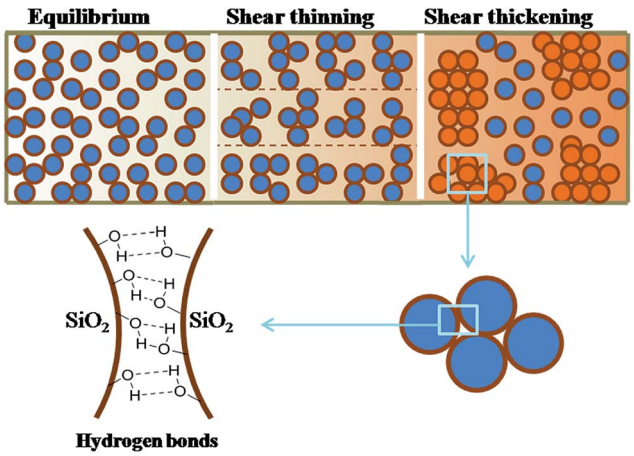

Scheme 2 The diagrammatic illustration of the change in microstructure for the transitions from equilibrium to shear thinning and shear thickening in the core–shell particle suspensions and the hydrogen bonding interactions at the surfaces of the particles.

The weight percentage of dispersed particles in the STFs was kept constant in this work. Due to the low average density of the SiO_2@PDA core–shell particles, the particles' volume ratio is larger than SiO_2. Under the same shear rate, the SiO_2@PDA core–shell particles must more easily form hydroclusters than the SiO_2 particles due to smaller inter-particles distances. Therefore, the critical shear rate for the SiO_2@PDA particle-based STFs was smaller than for the STF with SiO_2 particles. As shell thickness increased, the density further decreased. To this end, the critical shear rate increased with decreasing shell thickness. Moreover, more particles would be present in the thicker PDA shell-based STFs, thus the relative initial viscosity would increase. However, the weight percentage of PDA in the core–shell particles is very small (about 5 wt% for SiO_2@PDA-2). The number of the particles in the 62% SiO_2@PDA-2 STF was smaller than in the 72% SiO_2 STF, however it exhibited a better ST effect. Thus, increasing both the particle volume ratio and the surface interactions synergistically contributes to the enhancement of the ST effect. Here, the surface properties play a key role in determining the initial viscosity and the critical shear rate in the STF.

The hardness of the dispersed particles is also very important in the STFs because harder particles can resist larger forces without being broken.[25,27] It has been reported that the higher cross-linking density of PS-EA particles results in a better ST effect. For this SiO_2@PDA based STF, the hard SiO_2 enables the core–shell particles to form stable hydroclusters under application of an external shear force, thus exhibiting a large maximum viscosity. From the SEM and TEM images of pristine SiO_2 and the SiO_2@PDA nanospheres (Fig. 2 and Fig. S1†), we can observe that the surface of the SiO_2@PDA nanospheres clearly becomes rougher than that of pristine SiO_2. This result is consistent with previous reports.[41] Although the total amount of PDA in the coating is relatively small, the polymer layer is fluffy and the surface area of the nanospheres becomes larger as the roughness increases. With respect to discussions about the role

of friction forces in the shear thickening field, many works have been already been conducted.[60–66] Due to the increase in surface area and roughness of the SiO_2@PDA nanospheres compared with pristine SiO_2, the friction coefficient, μ, between the particles increases. Therefore, we speculate that particle–particle interactions increase simultaneously above a certain shear rate, which contributes to the stabilization of the hydroclusters. Based on above analysis, we can conclude that particles with hard cores and soft shells are an ideal candidates for use in high performance STFs. An optimum shell thickness can lead to the best ST effect in one system. The surface properties of the core–shell particles highly affect the interactions between particles, thus further influencing the relative ST effect.

4. Conclusions

In this work, a simple *in situ* polymerization method was introduced to scale-up the synthesis of core–shell SiO_2@PDA nanospheres, which can be used for preparing high performance STFs. The rheological properties of the synthesised STFs were highly dependent on the PDA shell thickness. With an increase in the shell thickness, the initial shear rate decreased and the maximum viscosity increased. Under optimum parameters, the maximum STF viscosity reached up to 194.6 Pa s. The SiO_2@PDA core–shell nanosphere-based STFs exhibited a better ST effect than naked SiO_2 and a possible enhancement mechanism was proposed. It was found that increasing the surface interactions plays a dominant role in determining the ST effect, while particle numbers and hardness can synergistically contribute to the enhancing the ST effect as well. This hard core/soft shell type composite particle-based STF will be useful in not only for fundamental studies, but also in engineering applications.

Acknowledgements

Financial support from the National Natural Science Foundation of China (Grant No. 11372301), the Fundamental Research Funds for the Central Universities and the National Basic Research Program of China (973 Program, Grant No. 2012CB937500) are gratefully acknowledged. This study was also supported by the Collaborative Innovation Center of Suzhou Nano Science and Technology.

References

1 E. Brown and H. M. Jaeger, *Rep. Prog. Phys.*, 2014, **77**, 46602.
2 E. Brown, N. A. Forman, C. S. Orellana, H. Zhang, B. W. Maynor, D. E. Betts, J. M. DeSimone and H. M. Jaeger, *Nat. Mater.*, 2010, **9**, 220–224.
3 R. Seto, R. Mari, J. F. Morris and M. M. Denn, *Phys. Rev. Lett.*, 2013, **111**, 218301.
4 H. A. Barnes, *J. Rheol.*, 1989, **33**, 329–366.
5 X. Z. Zhang, W. H. Li and X. L. Gong, *Smart Mater. Struct.*, 2008, **17**, 35027.
6 T. J. Kang, C. Y. Kim and K. H. Hong, *J. Appl. Polym. Sci.*, 2012, **124**, 1534–1541.
7 M. Soutrenon and V. Michaud, *Smart Mater. Struct.*, 2014, **23**, 35022.
8 C. Heussinger, *Phys. Rev. E: Stat., Nonlinear, Soft Matter Phys.*, 2013, **88**, 50201.
9 J. W. Bender and N. J. Wagner, *J. Colloid Interface Sci.*, 1995, **172**, 171–184.
10 D. P. Kalman and N. J. Wagner, *Rheol. Acta*, 2009, **48**, 897–908.
11 X. Cheng, J. H. McCoy, J. N. Israelachvili and I. Cohen, *Science*, 2011, **333**, 1276–1279.
12 B. J. Maranzano and N. J. Wagner, *J. Chem. Phys.*, 2002, **117**, 10291–10302.
13 R. Gamez-Corrales, J. Berret, L. M. Walker and J. Oberdisse, *Langmuir*, 1999, **15**, 6755–6763.
14 W. Jiang, Y. Sun, Y. Xu, C. Peng, X. Gong and Z. Zhang, *Rheol. Acta*, 2010, **49**, 1157–1163.
15 S. S. Shenoy and N. J. Wagner, *Rheol. Acta*, 2005, **44**, 360–371.
16 X. Q. Liu, R. Y. Bao and X. J. Wu, *RSC Adv.*, 2015, **5**, 18367–18374.
17 E. Brown, H. Zhang, N. A. Forman, B. W. Maynor, D. E. Betts, J. M. DeSimone and H. M. Jaeger, *Phys. Rev. E: Stat., Nonlinear, Soft Matter Phys*, 2011, **84**, 31408.
18 E. Brown, H. Zhang, N. A. Forman, B. W. Maynor, D. E. Betts, J. M. DeSimone and H. M. Jaeger, *J. Rheol.*, 2010, **54**, 1023–1046.
19 K. Yu, H. Cao, K. Qian, X. Sha and Y. Chen, *J. Nanopart. Res.*, 2012, **14**, 1–9.
20 G. V. Franks, Z. Zhou, N. J. Duin and D. V. Boger, *J. Rheol.*, 2000, **44**, 759–779.
21 A. Zupančič, R. Lapasin and G. Torriano, *Prog. Org. Coat.*, 1997, **30**, 79–88.
22 E. B. Bagley and D. D. Christianson, *J. Texture Stud.*, 1982, **13**, 115–126.
23 L. Chang, K. Friedrich, A. K. Schlarb, R. Tanner and L. Ye, *J. Mater. Sci.*, 2011, **46**, 339–346.
24 Y. Otsubo, M. Fujiwara, M. Kouno and K. Edamura, *Rheol. Acta*, 2007, **46**, 905–912.
25 D. P. Kalman, R. L. Merrill, N. J. Wagner and E. D. Wetzel, *ACS Appl. Mater. Interfaces*, 2009, **1**, 2602–2612.
26 A. Le Grand and G. Petekidis, *Rheol. Acta*, 2008, **47**, 579–590.
27 W. Jiang, F. Ye, Q. He, X. Gong, J. Feng, L. Lu and S. Xuan, *J. Colloid Interface Sci.*, 2014, **413**, 8–16.
28 S. Ullah, E. P. Ferreira-Neto, A. A. Pasa, C. C. Alcântara, J. J. Acuña, S. A. Bilmes, M. L. M. Ricci, R. Landers, T. Z. Fermino and U. P. Rodrigues-Filho, *Appl. Catal., B*, 2015, **179**, 333–343.
29 X. Liu, N. Wu and C. Cui, *RSC Adv.*, 2015, **5**, 24016–24022.
30 J. B. Li, S. J. Zhang and J. Liang, *RSC Adv.*, 2015, **5**, 7994–8001.
31 J. Feng, W. Qin and Y. Ju, *RSC Adv.*, 2015, **5**, 53514–53523.
32 J. T. McKeown, Y. Wu, J. D. Fowlkes, P. D. Rack and G. H. Campbell, *Adv. Mater.*, 2015, **27**, 1060–1065.
33 N. Iqbal, A. Afzal and A. Mujahid, *RSC Adv.*, 2014, **4**, 43121–43130.
34 Z. Li, A. Wang, C. Guo, Y. Tai and L. Qiu, *Dalton Trans.*, 2013, **42**, 13948–13954.
35 Y. J. Hong, M. Y. Son and Y. C. Kang, *Adv. Mater.*, 2013, **25**, 2279–2283.

36 D. Kim, Y. Tian and H. J. Choi, *RSC Adv.*, 2015, **5**, 81546–81553.
37 R. Ghosh Chaudhuri and S. Paria, *Chem. Rev.*, 2011, **112**, 2373–2433.
38 C. Jo, H. J. Lee and M. Oh, *Adv. Mater.*, 2011, **23**, 1716–1719.
39 R. Tayebee, M. M. Amini, H. Rostamian and A. Aliakbari, *Dalton Trans.*, 2014, **43**, 1550–1563.
40 M. L. Breen, A. D. Dinsmore, R. H. Pink, S. B. Qadri and B. R. Ratna, *Langmuir*, 2001, **17**, 903–907.
41 Z. Xia, Z. Lin, Y. Xiao, L. Wang, J. Zheng, H. Yang and G. Chen, *Biosens. Bioelectron.*, 2013, **47**, 120–126.
42 C. Jo, H. J. Lee and M. Oh, *Adv. Mater.*, 2011, **23**, 1716–1719.
43 Y. Ma, M. Qiao, C. Hou, Y. Chen, M. Ma, H. Zhang and Q. Zhang, *RSC Adv.*, 2015, **5**, 103064–103072.
44 R. Liu, Y. Guo, G. Odusote, F. Qu and R. D. Priestley, *ACS Appl. Mater. Interfaces*, 2013, **5**, 9167–9171.
45 Y. Hu, T. Zhao, P. Zhu, X. Liang, R. Sun and C. Wong, *RSC Adv.*, 2015, **5**, 58–67.
46 R. Palkovits, H. Althues, A. Rumplecker, B. Tesche, A. Dreier, U. Holle, G. Fink, C. H. Cheng, D. F. Shantz and S. Kaskel, *Langmuir*, 2005, **21**, 6048–6053.
47 K. Ohno, T. Morinaga, K. Koh, Y. Tsujii and T. Fukuda, *Macromolecules*, 2005, **38**, 2137–2142.
48 H. Sertchook and D. Avnir, *Chem. Mater.*, 2003, **15**, 1690–1694.
49 Y. P. Zhang, S. H. Lee, K. R. Reddy, A. I. Gopalan and K. P. Lee, *J. Appl. Polym. Sci.*, 2007, **104**, 2743–2750.
50 X. Xie, R. K. Li, Q. Liu and Y. Mai, *Polymer*, 2004, **45**, 2793–2802.
51 P. Xu, H. Wang, R. Lv, Q. Du, W. Zhong and Y. Yang, *J. Polym. Sci., Part A: Polym. Chem.*, 2006, **44**, 3911–3920.
52 S. X. Ma and S. L. Cooper, *J. Rheol.*, 2002, **46**, 339–350.
53 B. Chu, A. T. Brady, B. D. Mannhalter and D. R. Salem, *J. Phys. D: Appl. Phys.*, 2014, **47**, 335302.
54 H. Lee, S. M. Dellatore, W. M. Miller and P. B. Messersmith, *Science*, 2007, **318**, 426–430.
55 L. Zongguang, Q. Shuxin and W. Jie, *Progress in Chemistry*, 2015, **27**, 212–219.
56 C. Ho and S. Ding, *J. Biomed. Nanotechnol.*, 2014, **10**, 3063–3084.
57 S. R. Raghavan, H. J. Walls and S. A. Khan, *Langmuir*, 2000, **16**, 7920–7930.
58 F. J. Galindo-Rosales and F. J. Rubio-Hernandez, *Appl. Rheol.*, 2010, **20**, 22781–22787.
59 J. Warren, S. Offenberger, H. Toghiani, C. U. Pittman Jr, T. E. Lacy and S. Kundu, *ACS Appl. Mater. Interfaces*, 2015, **7**, 18650–18661.
60 R. Mari, R. Seto, J. F. Morris and M. M. Denn, *J. Rheol.*, 2014, **58**, 1693–1724.
61 L. E. Silbert, D. Ertaş, G. S. Grest, T. C. Halsey and D. Levine, *Phys. Rev. E: Stat., Nonlinear, Soft Matter Phys.*, 2002, **65**, 31304.
62 M. Jerkins, M. Schröter, H. L. Swinney, T. J. Senden, M. Saadatfar and T. Aste, *Phys. Rev. Lett.*, 2008, **101**, 18301.
63 L. E. Silbert, *Soft Matter*, 2010, **6**, 2918–2924.
64 C. Heussinger, *Phys. Rev. E: Stat., Nonlinear, Soft Matter Phys.*, 2013, **88**, 50201.
65 R. Seto, R. Mari, J. F. Morris and M. M. Denn, *Phys. Rev. Lett.*, 2013, **111**, 218301.
66 N. Fernandez, R. Mani, D. Rinaldi, D. Kadau, M. Mosquet, H. Lombois-Burger, J. Cayer-Barrioz, H. J. Herrmann, N. D. Spencer and L. Isa, *Phys. Rev. Lett.*, 2013, **111**, 108301.